

# Optical Characterization of MEMS Deformable Mirror Array Structures

Soe-Mie F. Nee<sup>\*a</sup>, Lewis F. DeSandrea<sup>a</sup>, Thomas Bifano<sup>\*\*b</sup>, Linda F. Johnson<sup>a</sup> and Mark B. Moran<sup>a</sup>

<sup>a</sup>Research Department, Naval Air Warfare Center Weapons Division;

<sup>b</sup>Dept. of Manufacturing Engineering, Boston University

## ABSTRACT

Surface properties and optical properties of several deformable mirror arrays (DMA) without actuators were characterized. The mirror arrays are micro-electronic-mechanical system (MEMS) devices which were fabricated by Boston University for wavefront correction in adaptive optics. The surface properties measured for the samples agree with the properties specified for the BU-MEMS-DMA structures. Scattering and diffraction by the mirror arrays were measured at a wavelength of 632.8 nm. The DMA with the etching pattern generates a diffraction pattern full of special structures. The broadening is serious for a rough sample while it is negligible for a smooth continuous membrane DMA. The diffraction pattern demonstrates that the DMA with an rms roughness of 300 nm is not suitable for the adaptive optics to correct for wavefront error. The continuous membrane DMA with roughness less than 10 nm are useful for adaptive optics.

Keywords: Diffraction, scattering, MEMS, mirror array, adaptive optics, surface profiles.

## 1. INTRODUCTION

Imaging sensors in high speed vehicles suffer from errors due to atmospheric turbulence, aerodynamic turbulence, and aero-thermal heating of the sensor window. Boston University (BU) has developed a new class of silicon based deformable mirror array (DMA) that are capable of correcting time-varying aberrations in imaging or beam forming applications.<sup>1-6</sup> The prototype device of DMA is compact, light-weight and as small as a dime. Each mirror is composed of a flexible silicon membrane supported by an underlying array of electrostatic actuators. All structural and electronic elements were fabricated through conventional surface micro-machining using polycrystalline silicon thin films. The MEMS-DMA adaptive optics (AO) devices hold the promise of an inexpensive, low power, compact, high performance alternative to existing designs. The emergence of MEMS-based DMA is likely to extend the field of AO from large astronomical systems to ship, aircraft and high speed vehicles where aberration correction is necessary in order to improve optical imaging. The next generation sensors will benefit from improved imaging performance in the presence of severe wavefront distortions due to atmospheric or aero-dynamic induced optical aberrations. Naval Air Warfare Center (NAWC) have characterized a segmented MEMS-DMA sample which was then coated with gold.<sup>7</sup> The gold coating changed the sample surface profile entirely, and the scattering was measured only after the coating. Data were too few to draw any conclusion. More DMA samples were tested afterward. This paper reports the results of the measured scattering, diffraction and surface properties of these DMA samples. Section 2 describes the sample specifications. Section 3 gives the measured surface properties. Section 4 reports the measured scattering and diffraction pattern. Section 5 relates the diffraction pattern to the surface properties and concludes the paper.

## 2. MEMS DEFORMABLE MIRROR ARRAYS

The specifications of the BU-MEMS-DMA device are listed in Table 1 as compared with the industrial standard macroscopic DMA. The actuator stroke is the maximum vertical displacement at the center of a mirror when an actuator voltage is applied. The advantages of the BU-MEMS-DMA are its small size, light weight, fast response and low power consumption. The look of such a device is shown in Fig. 1. BU has fabricated three types of MEMS-DMA as shown in Fig. 2: (a) continuous membrane mirror on actuators, (b) segmented mirrors with piston motion, (c) segmented mirrors having tip-tilt motion. Individual micro-mirrors of silicon are deformable with adjustable heights, and those that are

---

\* neesf@navair.navy.mil; phone 760-939-1425; fax 760-939-6593; U.S. Naval Air Warfare Center Weapons Division, Research Department, Code 4T4100D, China Lake, CA 93555-6001.

\*\* Bifano@bu.edu; phone 617-353-5619; fax 617-353-5548; Boston University, Manufacturing Engineering Department, 15 Saint Marys St., Brookline, MA 02446.

segmented with tip-tilt freedom allow adjustment in the phase of a wavefront. Two MEMS-DM array samples were tested: Sample A with continuous membrane and Sample B with segmented mirrors. Sample B has 10x10 mirror sections in a square of 3 mm x 3 mm, and Sample A has 140 actuators with the actuator configuration as 12x12 square grid without corners in an area of 3.3 mm x 3.3 mm. Since silicon mirror does not reflect in the midwave infrared (MWIR), Sample B was coated with gold in order to see whether it can be applicable in MWIR. Sample B after coating is called Sample E.

Table 1. Comparison of BU-MEMS-DM with the industry-standard macroscopic DMA.

Specification	BU MEMS DMA	Macroscopic DMA
Number of actuators	10x10, 140	37, 97, or 350
Actuation	Integrated electrostatic	External piezoelectric
Package size	10 cc	1000 cc
Power consumption	0.001 Watts/actuator	7 watts/actuator
Actuator spacing	0.3 mm	7 mm
Actuator stroke	2 $\mu$ m	4 $\mu$ m
Hysteresis	0 %	> 5 %
Settling time	0.2 ms	15 ms
Static surface roughness	35 nm ra	30 nm ra

### 3. SURFACE TOPOGRAPHY

Three-dimensional surface profiles of the MEMS mirror arrays were taken using a Wyko interferometric profiler. The surface topography of Sample B was also measured using a Nomarski microscope. Figure 3a is a 50x micrograph showing the look of the silicon mirror array, and Fig. 3b shows a detail structure of a single mirror with 200x magnification. Other samples look similar to Fig. 3 under the microscope. Each mirror section has an area of 0.3 mm x 0.3 mm, and each segmented mirror has an area of 0.24 mm x 0.24 mm. The etching holes are 30  $\mu$ m apart. The gap between two mirror sections is about 6.8  $\mu$ m as measured by a stylus profiler for Sample E.

Figure 4a shows a three-dimensional (3d-) profile  $z(x,y)$  for a section of 3x3 mirror array for Sample A, and Fig. 4b is a two-dimensional (2d-) profile  $z(x)$  at a fixed y-position of the 3d-profile as measured by a Wyko interferometric profiler. Sample A of continuous membrane type is pretty smooth, and the roughness is due to the etching holes and the dividing troughs. Figures 5 and 6 show the similar Wyko surface profiles for Samples B and E correspondingly. Table 2 lists the type, root-mean-square (rms) roughness and average absolute (ra) roughness of these samples obtained by a WYKO profiler. The roughnesses in Table 2 are the average over the measured values for several 3x3 array sections. Sample B as shown by Fig. 5 is also smooth, and each segmented mirror sags to the center, agreed with the deformable pattern simulated in Ref. [2]. The etching holes are visible in the 2d-profiles of these smoother samples. Sample E is the sample after gold coating on Sample B. The coating is 200 nm thick. This coating has change the rms roughness from 18 nm to 300 nm and the ra roughness from 8 nm to 227 nm. Some of the mirrors in Sample E were crushed by the heavy gold coating so that their profiles do not look like the normal bell shape as those shown in Fig. 6.

Table 2. Roughness of MEMS-DMA samples of different types measured using a WYKO profiler.

Sample	Type	Rms Roughness (nm)	Ra Roughness (nm)
A	Continuous	8.7	6.5
B	Segmented	18	8
E	Segmented + gold coating	300	227

### 4. DIFFRACTION PATTERNS

The NAWCWD ellipsometer was modified to measure the diffraction patterns of the MEMS-DMA samples.<sup>8</sup> The ellipsometer was fabricated by UDRI in 1983.<sup>9</sup> The schematics of the modified precision system for diffraction measurement is shown in Fig. 7. The HeNe laser has a wavelength ( $\lambda$ ) of 633 nm and a beam-width of 1.6 mm. It was originally designed as the aligning beam for the ellipsometer. The chopper coupled with a lock-in amplifier was used to suppress the ambient noise. The polarizer was set at 45°. The detecting direction was at 90° to the incident beam, and the angle of incidence was varied during the measurement. The precision of the incident angle is 0.01°, and the acceptance angle spanned by the slit in front of the detector from the sample is 0.014° for Sample A and 0.035° for Sample E. For no sample, the incident beam profiles for both cases are shown in Fig. 8. The incident beam profiles show a little diffraction

pattern because the laser has passed through the grating monochromator. A wider slit gives more intensity and slightly wider beam width in the measurement. The diffraction patterns of Samples A and E were tested. Because Sample B with the original segmented mirrors was gold-coated to Sample E, diffraction pattern for Sample B is not available.

By using the off-specular angle (  $OSA \equiv \theta_{out} - \theta_{in}$  ) as the abscissa where  $\theta_{in}$  and  $\theta_{out}$  are the angles of incidence and diffraction respectively,<sup>8</sup> the sample diffraction pattern can be compared with the incident beam profile. Figure 9a and 9b shows the diffraction pattern on the plane of incidence for Samples A and E respectively, as compared with the incident beam profile. These figures show that the reflected beam was broadened with bright and dark fringes imposed on it and its peak intensity was reduced. To see better the broadening effects, Figs. 8 were replotted as Fig. 10 using the relative intensity as the ordinate. The relative intensity is normalized to 1 at the specular direction. The incident beam profiles for both cases of Fig. 8 overlap in Fig. 10. The broadening effect is serious for Sample E while it is negligible for Sample A. This means that Sample A can be used as an adaptive optics device while Sample E is not useful for AO purpose because the roughness of Sample E is too large. We will analyze the interesting diffraction pattern of Sample E for which a wider pattern was measured.

To analyze the diffraction pattern of a sample, we examine the phase change  $\Delta\delta$  between the outgoing beam and the incident beam. The phase change is

$$\Delta\delta = (\sin \theta_{out} - \sin \theta_{in}) 2\pi \Delta x / \lambda = 2\pi \eta \Delta x / \lambda ,$$

where  $\Delta x$  is a characteristic length of the surface,  $\lambda$  is the wavelength, and  $\eta$  is defined by<sup>10</sup>

$$\eta \equiv \hat{x} \cdot (\mathbf{k}_{out} - \mathbf{k}_{in}) \lambda / 2\pi = \sin \theta_{out} - \sin \theta_{in} .$$

As  $\Delta\delta$  is changed by  $2\pi$ , we have a fringe. The  $\Delta\eta$  for a fringe or a group of fringes is equal to  $\lambda/\Delta x$ . It is convenient to express  $\eta$  in degree as

$$\eta \text{ (deg)} = (\sin \theta_{out} - \sin \theta_{in}) 180^\circ/\pi$$

because it is on the same order of OSA and easier to understand. We use  $\eta$  as the abscissa and the relative BRDF as the ordinate in a plot of diffraction pattern. The relative BRDF is obtained by dividing the intensity by  $\cos \theta_{out}$  and then normalizing to 1 at the specular. Using BRDF rather than the direct measured intensity makes the height of the two arms of the pattern more balancing.

Figure 10 shows the relative BRDF plotted against  $\eta$  for Sample E. With  $\eta$  as the abscissa, there are about 16.5 fringes in a  $\Delta\eta = 2^\circ$  for the whole range of Fig. 11. There are a total of 107.5 fine fringes for  $\eta$  from  $-7$  to  $6^\circ$ . The spacing for a fringe is  $\Delta\eta = 0.1209^\circ$  which corresponds to  $\Delta x = 299.9 \mu\text{m}$ , the repeated length for the mirror array. Table 3 shows the characteristic lengths correspond to different features of the diffraction pattern. The second sidelobes gives a  $\Delta x$  of  $29.9 \mu\text{m}$  which is the distance between two adjacent etching holes. The center lobe plus the two first side lobes contain 44 fringes corresponds to  $6.82 \mu\text{m}$  which is the width of the gap between the mirror sections. The beats gives  $\Delta x = 53.2 \mu\text{m}$  which is equal to the distance between two adjacent mirrors ( $60 \mu\text{m}$ ) minus the width ( $6.8 \mu\text{m}$ ) of the gap which dividing the two mirror sections. The surface topography rich of special structures give rise to the diffraction pattern also rich of special structures. The serious diffraction by a mirror array of poor optical quality hurts fatally the performance of a deformable mirror to correct for wavefront distortion. The continuous membrane DMA with roughness less than  $10 \text{ nm}$  such as Sample A are better candidates for adaptive optics.

Table 3. Features of diffraction pattern for a BU-MEMS mirror array (Sample E).

Type	Fringes	$\Delta\eta$ ( $^\circ$ )	$\Delta x$ ( $\mu\text{m}$ )
Fine structure	1	0.1209	299.9
Beats	5.75	0.695	53.19
Center lobe	19	2.2768	15.9
First side lobe	12.5	1.52	23.9
Second side lobe	10	1.213	29.9
Center + 1st side lobes	44	5.3165	6.82

## 5. SUMMARY

Surface properties and optical properties of several MEMS deformable mirror arrays without actuator fabricated by Boston University were characterized. The micrographs and the interferometric profiles measured for the original delivered samples agree with the properties specified for the BU-MEMS-DMA. The delivered silicon segmented mirror array was then coated with gold in order to be applicable to the midwave infrared. The profiles are very different between the samples before and after the coating and the surface roughness was increased to 28 times the original after the coating. The mirror arrays with the wiring pattern generates a diffraction pattern full of special structures. The broadening is serious for the rough coated sample while it is negligible for the smooth continuous membrane DMA. The diffraction pattern demonstrates that the DMA with an rms roughness of 300 nm is not suitable for the adaptive optics to correct for wavefront error. The continuous membrane DMA with roughness less than 10 nm are useful for adaptive optics.

## ACKNOWLEDGEMENT

This research was supported partially by the Science and Technology Program and the In-house Laboratory Independent Research Program of the Naval Air Warfare Center Weapons Division at China Lake, California.

## REFERENCES

1. R. K. Mali, T. G. Bifano, N. Vandelli, and M. N. Horenstein, "Development of microelectromechanical deformable mirrors for phase modulation of light," *Opt. Eng.* **36**, pp. 542-548, 1997.
2. T. G. Bifano, R. K. Mali, J. K. Dorton, J. Perreault, N. Vandelli, M. N. Horenstein, and D. A. Castanon, "Continuous-membrane surface-micromachined silicon deformable mirror," *Opt. Eng.* **36**, pp. 1354-1360, 1997.
3. T. G. Bifano, J. Perreault, R. K. Mali, and M. N. Horenstein, "Microelectromechanical deformable mirrors," *J. Selected Topics Quan. Electro.* **5**, pp. 83-90, 1999.
4. R. K. Mali, T. G. Bifano, and D. A. Koester, "Design-based approach to planarization in multilayer surface micromachining," *J. Micromech. Microeng.* **9**, pp. 294-299, 1999.
5. M. Horenstein, T. G. Bifano, S. Pappas, J. Perreault, and R. K. Mali, "Real time optical correction using electrostatically actuated MEMS devices," *J. Electrostatics* **46**, pp. 91-1-1, 1999.
6. M. Horenstein, T. G. Bifano, R. K. Mali, and N. Vandelli, "Electrostatic effects in micromachined actuators for adaptive optics," *J. Electrostatics* **42**, pp. 69-82, 1997.
7. L. DeSandre, S.-M. Nee, L. Johnson, M. Moran, and T. Bifano, "What's new at China Lake: Optical characterization of novel microelectronic mechanical system adaptive optic array structure," *Spectral Reflections* **30(2)**, pp.11-14, 2000.
8. S.-M. F. Nee and T. W. Nee, "Polarization of scattering by rough surfaces," in *Scattering and Surface Roughness*, Z. Gu and A. A. Maradudin, eds., *Proc. SPIE* **3426**, pp. 169-180, 1998.
9. T. A. Leonard, J. Loomis, K. G. Harding, and M. Scott, "Design and construction of three infrared ellipsometers for thin film research," *Opt. Eng.* **21**, pp. 971-975, 1982.
10. S.-M. F. Nee, R. V. Dewees, T.-W. Nee, L. F. Johnson and M. B. Moran, "Slope distribution of a rough surface measured by transmission scattering and polarization," *Appl. Opt.* **39**, pp. 1561-1569, 2000.

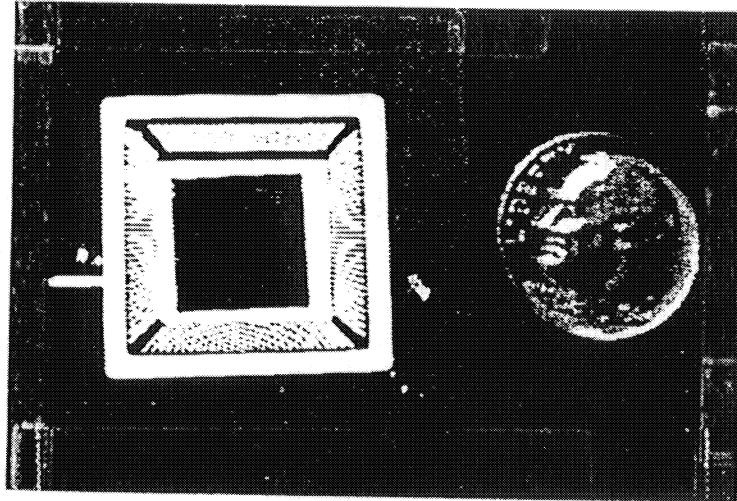


Fig. 1: Picture of a BU-MEMS-DMA device.

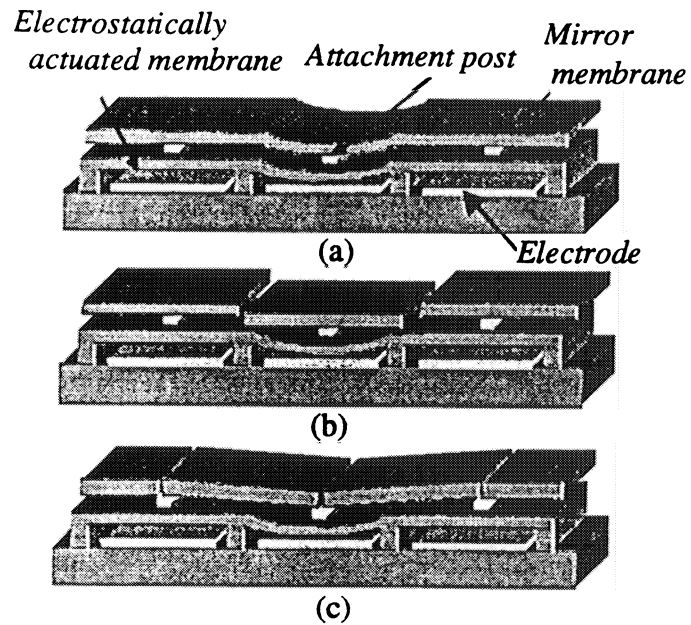
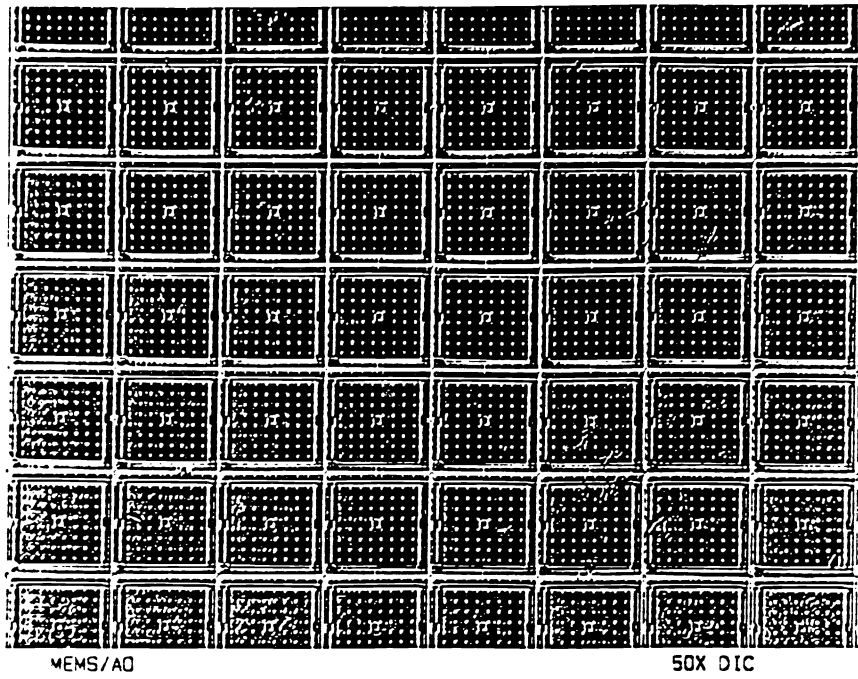


Fig. 2: Boston University has fabricated three types of MEMS-DMAs: (a) continuous membrane mirror on actuators, (b) segmented mirrors with piston motion, (c) segmented mirrors having tip-tilt motion.

(a)



(b)

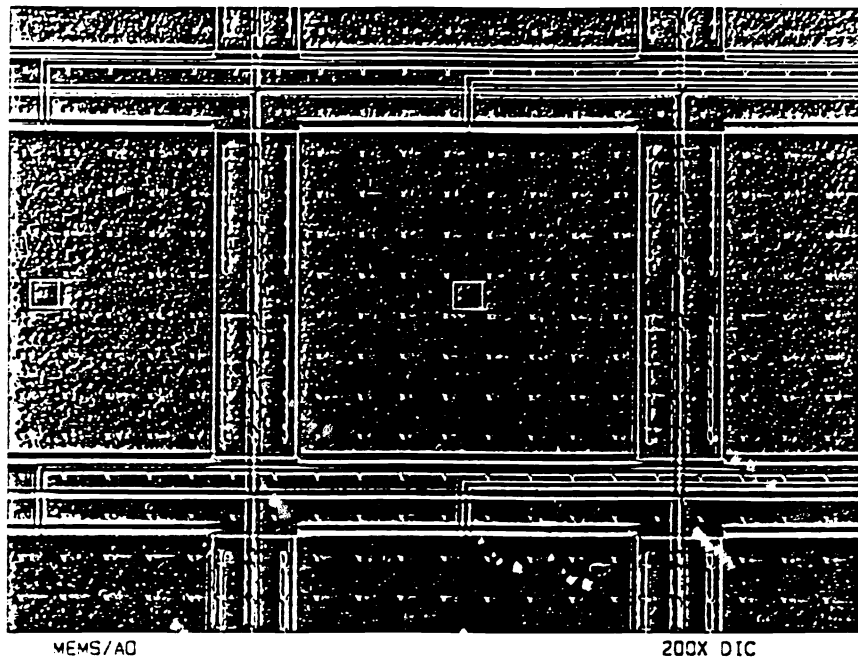
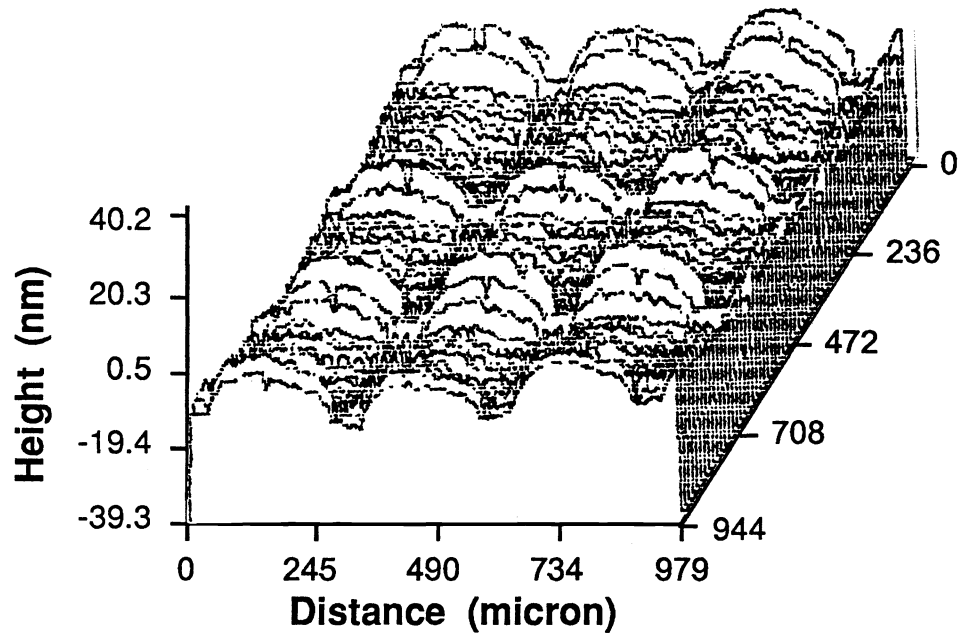


Fig. 3: (a) A 50x micrograph showing the look of the silicon mirror array, (b) a detail structure of a single mirror with 200x magnification.

(a)



(b)

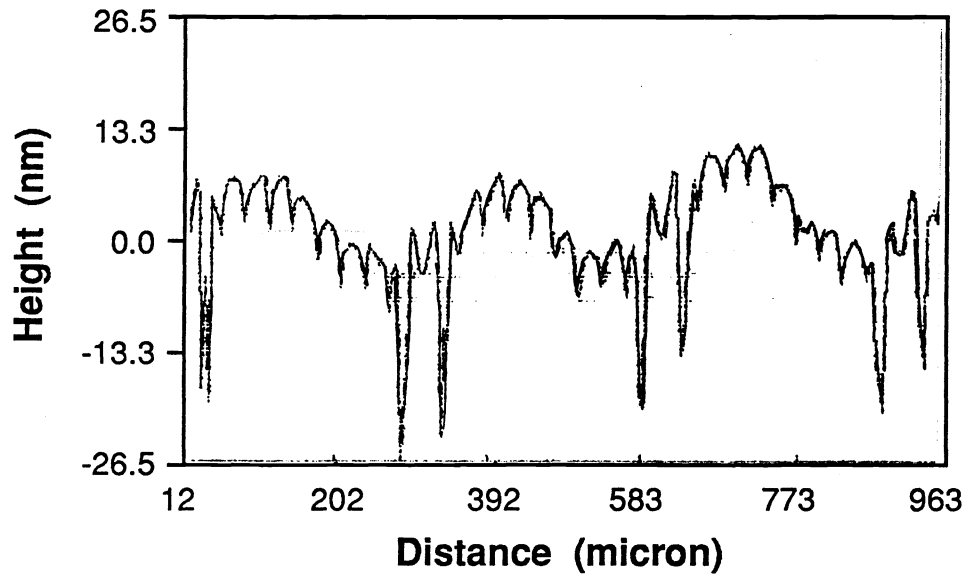


Fig. 4: Surface profiles taken using a WYKO interferometric profiler for Sample A: (a) a 3d-profile for a section of 3x3 mirrors, (b) a 2d-profile near the center of the 3d-profile. Sample A has continuous membrane mirrors.

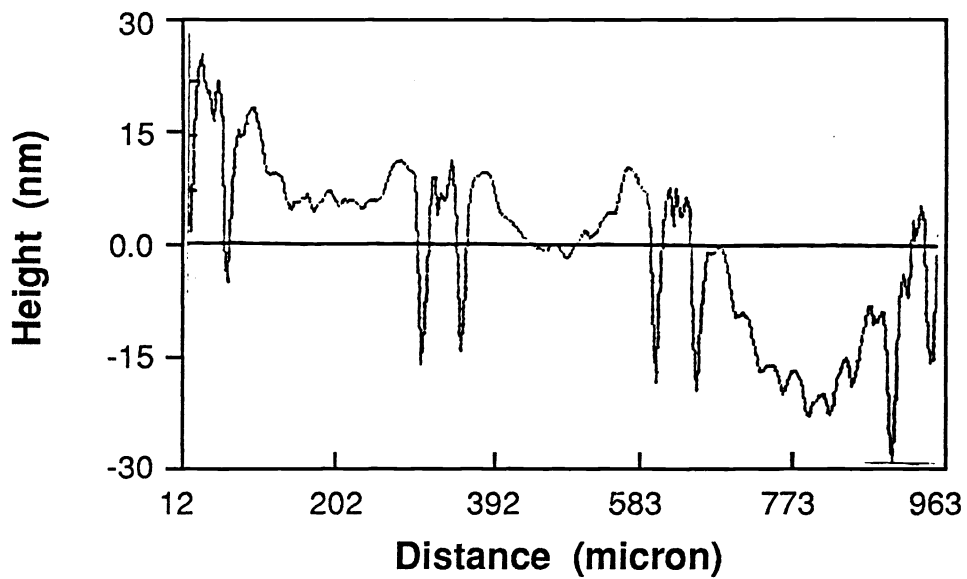
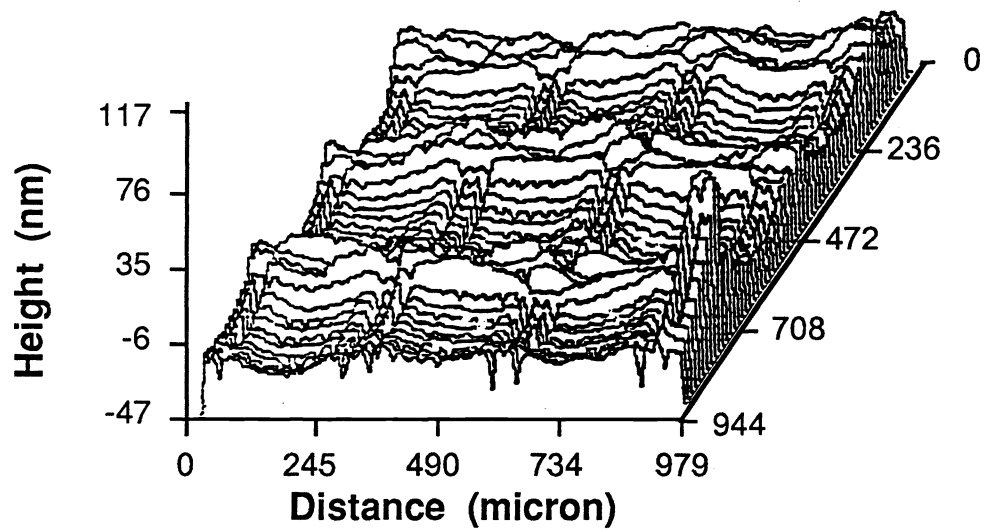


Fig. 5: 3d- and 2d-surface profiles for the segmented mirrors of Sample B. Roughness of Sample B is comparable to Sample A.

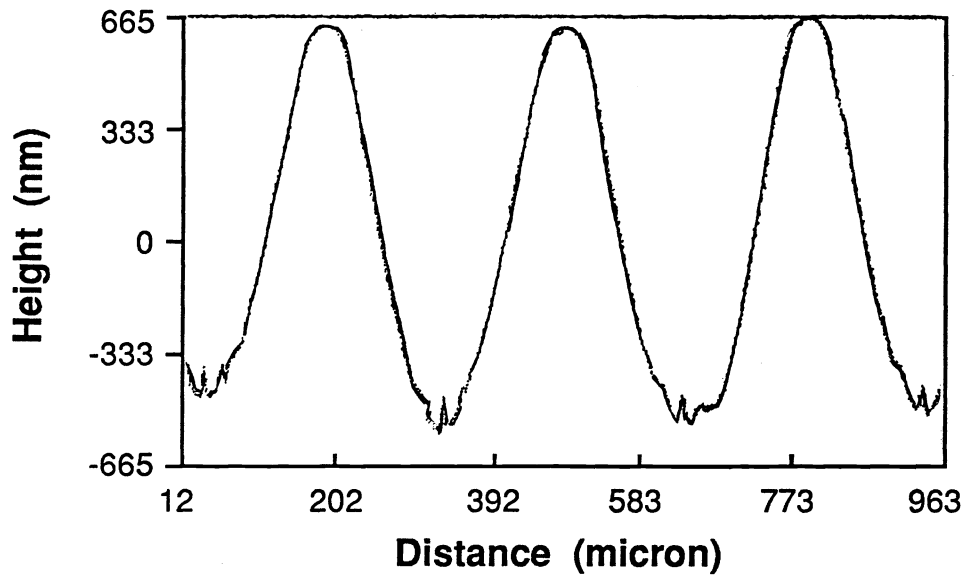
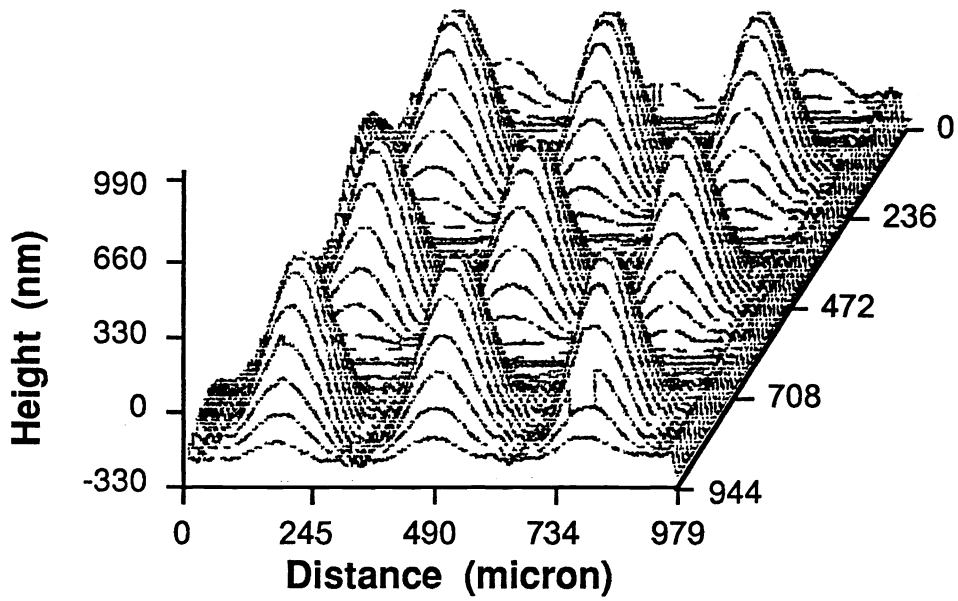


Fig. 6: 3d- and 2d-surface profiles for Sample E which is after the gold-coating on Sample B. Roughness of Sample E is much higher than Sample B.

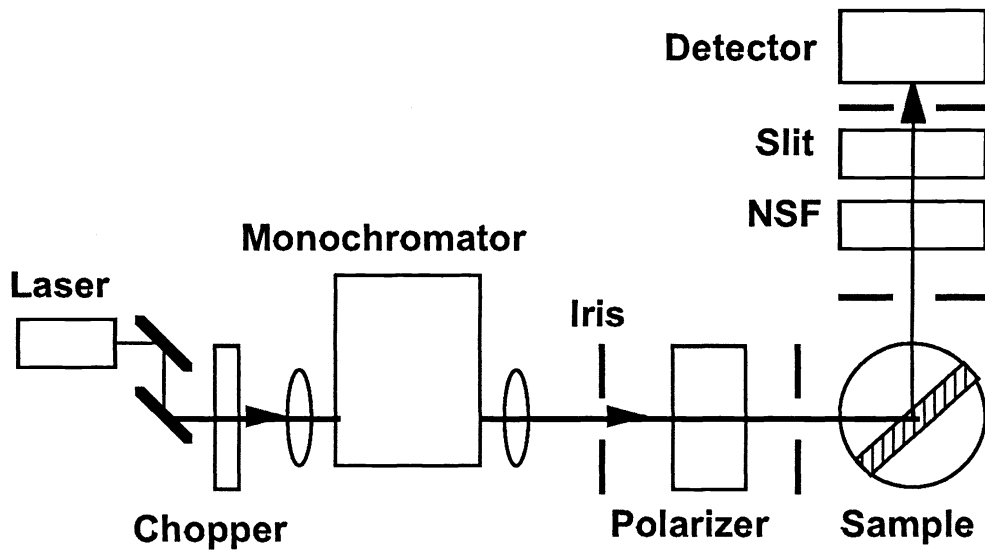


Fig. 7: The schematics of the precision diffraction measurement system.

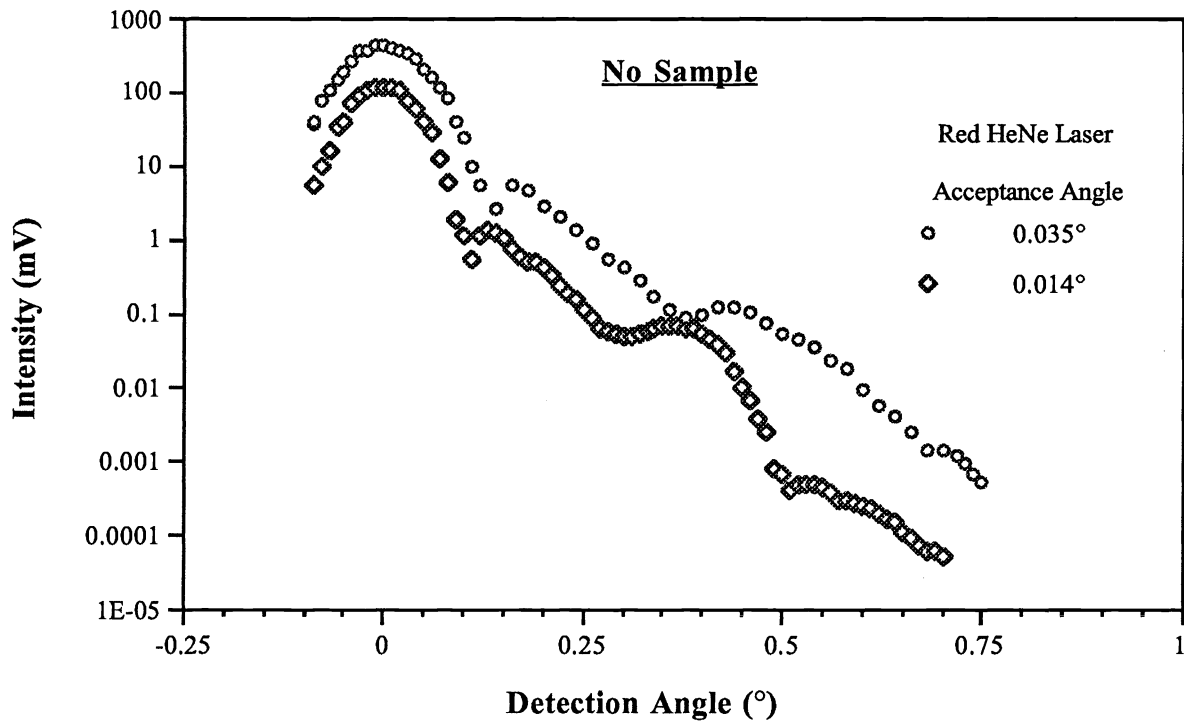


Fig. 8: Incident beam profiles for acceptance angles of 0.014° and 0.035°.

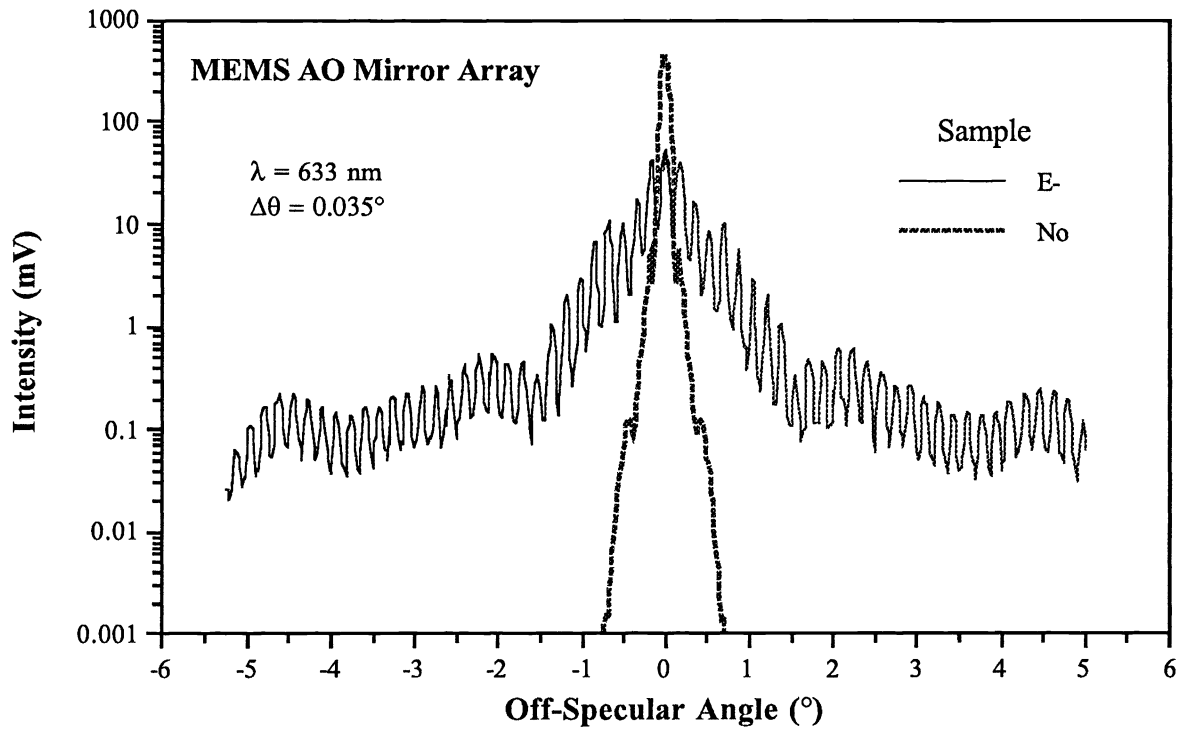
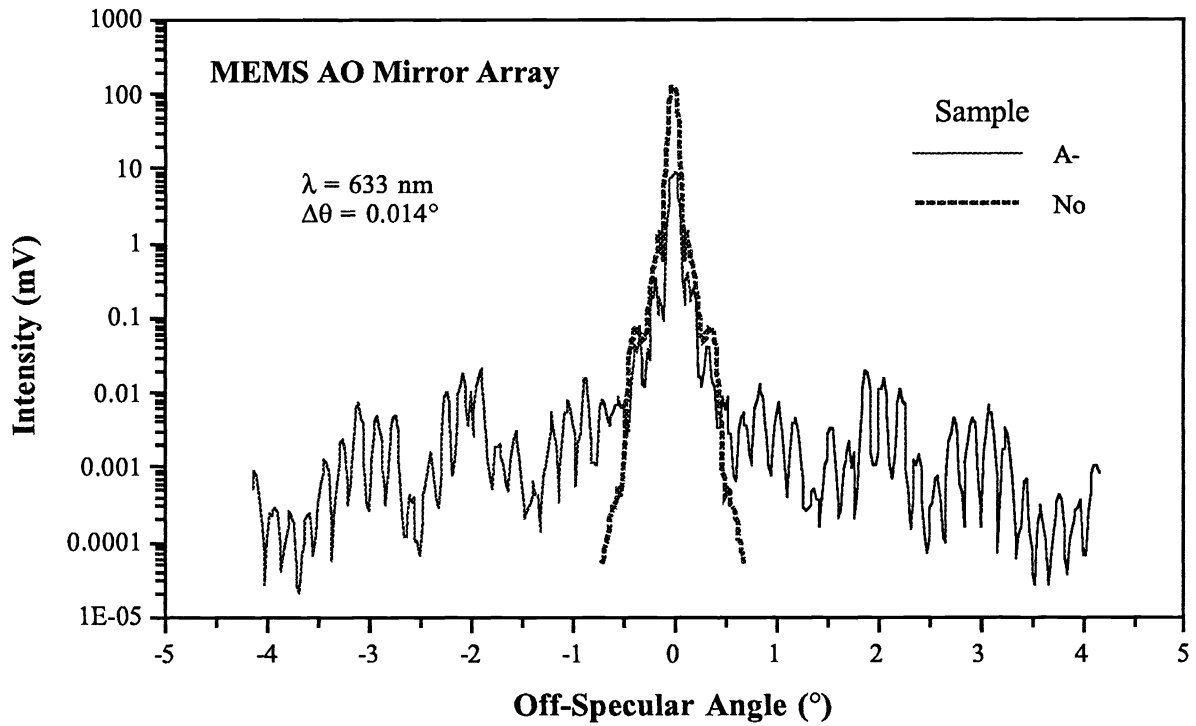


Fig. 9: Measured intensity versus OSA for diffraction on the plane of incidence for (a) Samples A with an acceptance angle of  $0.014^\circ$  and (b) Sample E with an acceptance angle of  $0.035^\circ$ , as compared with the incident beam profiles.

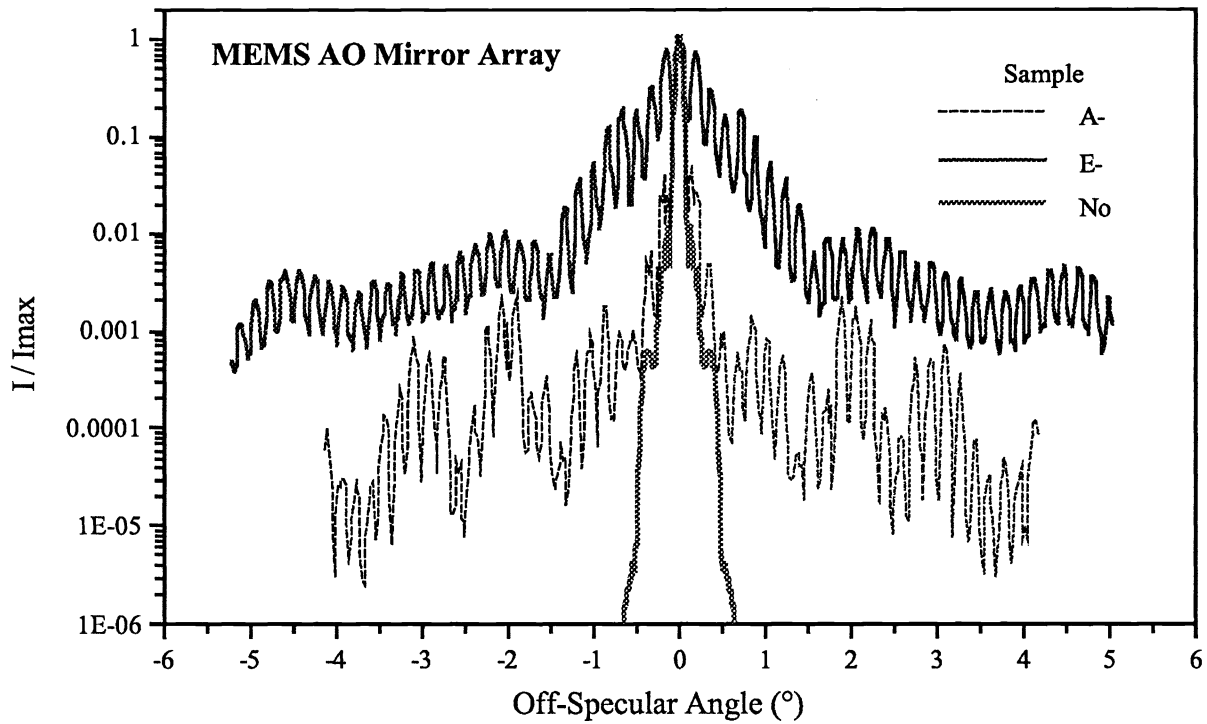


Fig. 10: Relative intensity versus OSA for diffraction by Samples A and E as compared with the incident beam profile. The relative intensity is normalized to 1 at the specular direction.

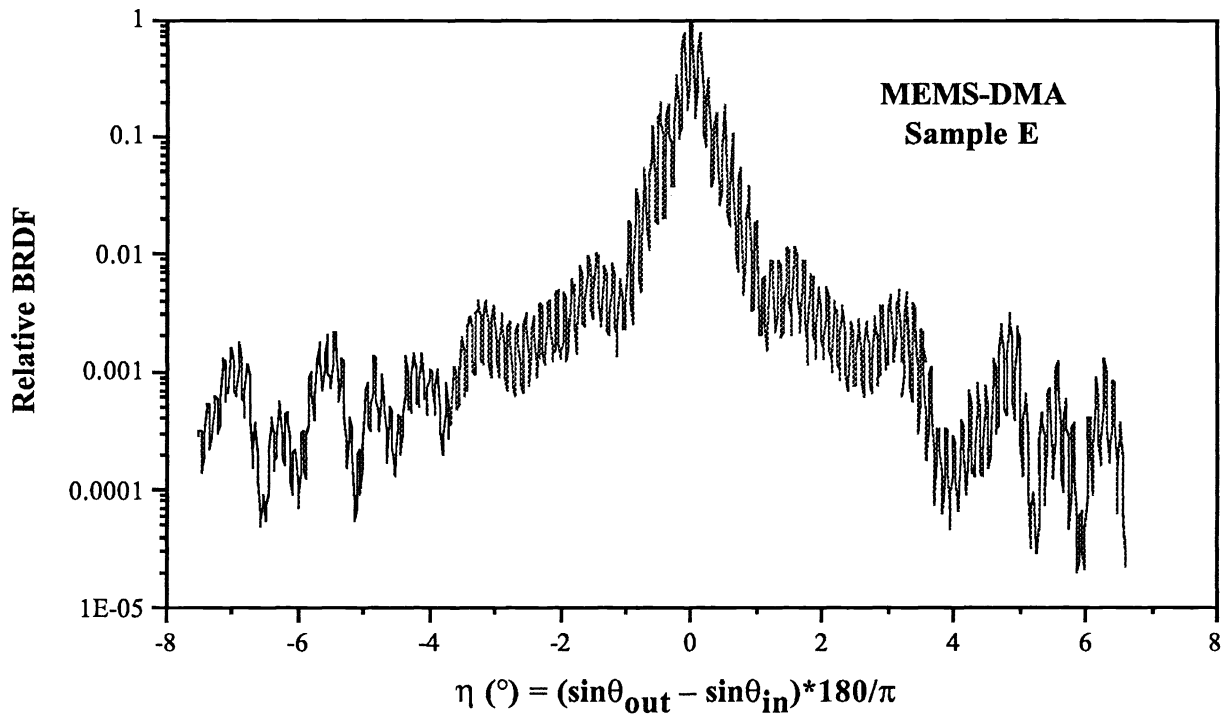


Fig. 11: Relative BRDF plotted against  $\eta$  in degree for Sample E. The relative BRDF is normalized to 1 at the specular direction.